Research Article Vol. 15, No. 12 / 1 Dec 2024 / Biomedical Optics Express 6670
Biomedical Optics EXPRESS

Simultaneous 2-photon and 3-photon excitation with a red fluorescent protein-cyanine dye probe pair in the 1700-nm excitation window for deep *in vivo* neurovascular imaging

Fei Xia,[1,2,3] David Sinefeld,[1,4] Zong Chang,[5] Xiaojing Gong,[5,6] and Qinchao Sun[5,7]

[1]*School of Applied and Engineering Physics, Cornell University, Ithaca, New York, USA*
[2]*Meinig School of Biomedical Engineering, Cornell University, Ithaca, New York, USA*
[3]*Present address: Laboratoire Kastler Brossel, ENS-PSL Research University, CNRS, Sorbonne Université, Collège de France, Paris, France*
[4]*Present address: Department of Applied Physics and Electro-Optical Engineering, Jerusalem College of Technology, Jerusalem, Israel*
[5]*Guangdong Provincial Key Laboratory of Biomedical Optical Imaging Technology, Center for Biomedical Optics and Molecular Imaging, Shenzhen Institute of Advanced Technology, Chinese Academy of Sciences, Shenzhen 518055, China*
[6]*xj.gong@siat.ac.cn*
[7]*Qchao.sun@siat.ac.cn*

Abstract: *In vivo* imaging of the neurovascular network is considered to be one of the most powerful approaches for understanding brain functionality. Nevertheless, simultaneously imaging the biological neural network and blood vessels in deep brain layers in a non-invasive manner remains to a major challenge due to the lack of appropriate labeling fluorescence probe pairs. Herein, we proposed a 2-photon and 3-photon fluorescence probe pair for neurovascular imaging. Specifically, the red fluorescence protein (RFP) with an absorption maximum of around 550 nm is used as a 3-photon excited probe to label neurons, and a cyanine derivative dye Q820@BSA has a NIR absorption maximum of 825 nm as a 2-photon excited probe to label the vasculature, enabling single wavelength excitation at 1650 nm for neurovascular imaging with high emission spectral separation (>250 nm). In particular, the 2-photon action cross-section of Q820@BSA was found to be about 2-fold larger than that of indocyanine green (ICG), a commonly used red 2-photon fluorescence labeling agent, at the same excitation wavelength. Benefiting from the long wavelength advantage in reducing scattering in both 2 and 3-photon excitation of the fluorescence pairs, we demonstrated *in vivo* neurovascular imaging in intact adult mouse brains through white matter and deep into the hippocampus in the somatosensory cortex.

1. Introduction

Recognized as one of the most intricate and intelligent systems on Earth, the neurovascular network has been at the center of extensive scientific efforts aimed at understanding its complex mechanisms of communication and cooperation [1–4]. It has been discovered that there is a profound coordination between neural activity and vascular function. A prominent example of this relationship is neurovascular coupling (NVC), a process whereby capillary blood flow is modulated by neural activity [1,2,5,6]. In the quest to elucidate NVC, *in vivo* imaging techniques have proven indispensable. Functional MRI, which exploits the coupling between neuronal activity and brain hemodynamics, facilitates non-invasive localization and measurement of brain activity [7]. However, while functional MRI can provide large-scale *in vivo* brain images, it is constrained by its limited spatial resolution. Conversely, *in vivo* optical fluorescence microscopy

#534688 https://doi.org/10.1364/BOE.534688
Journal © 2024 Received 8 Jul 2024; revised 18 Oct 2024; accepted 18 Oct 2024; published 5 Nov 2024

Biomedical Optics EXPRESS

has been developed to visualize biological processes with superior spatial and temporal resolutions [8]. Despite these advancements, the technique is challenged when imaging deeper within highly scattered tissues while maintaining high spatial resolution. A variety of innovative imaging techniques, primarily employing long-wavelength excitation to diminish tissue scattering, have been proposed to overcome this limitation [9–11]. Among these innovations is the short-wave infrared (SWIR) one-photon fluorescence imaging, developed to leverage the advantages of long emission wavelengths for deep *in vivo* tissue imaging [12]. Moreover, long wavelength/SWIR 2-photon and 3-photon fluorescence imaging have been utilized for *in vivo* 3D deep mouse brain imaging via long-wavelength excitation [13,14].

For long wavelength fluorescence microscopy, reliable and bright fluorescent probes are essential for intravital deep imaging for biological studies [15]. For instance, the toolbox development of fluorescence protein makes the *in vivo* labeling neuron network feasible [16]. Thanks to the significant 3-photon action cross-section of fluorescence proteins, *in vivo* 3-photon imaging of the fluorescence protein labeled neural imaging has been demonstrated reaching over 1 mm in deep mouse brain, covering all the cortical layers [13,14]. However, in comparison to fluorescent protein, small organic fluorescent molecules possess unique advantages, including easy modification of their photophysical properties and molecular structures. Specifically, the cyanine dyes are one of the most studied fluorescent probes for imaging. For example, ICG, a candidate from the cyanine dyes family, is the only FDA-approved dye with an emission spectrum greater than 800 nm [15]. It has been widely used in ophthalmology for angiography and in other fields for assessing blood flow. While ICG's 2-photon action cross section is sufficient for imaging at shallower depths [17], going deeper in the brain requires a dye with higher brightness and a larger 2-photon cross section, excited within the optimal imaging window, to achieve a stronger signal and better imaging quality in highly scattering tissues.

It was demonstrated that the optimal imaging windows for mouse brain imaging are around 1300 nm and 1700nm, where 1700nm being most promising for deeper mouse brain imaging [11,18–20]. 3-photon fluorescence imaging of RFP labeled neurons has been reported for deep brain tissue with 1700nm excitation [13]. To image blood vessels with 3-photon excitation, red fluorophores such as Texas Red have been employed to label the vasculature [13]. Due to the strong spectral overlap of red fluorophores (such as RFP and Texas Red), simultaneous deep imaging of the neurovascular system is challenging, and particularly has not been demonstrated with 1700nm excitation. Thus, there is a need to identify proper labeling fluorescence probe pairs that allow sufficient spectral separation to avoid spectral crosstalk using 1700nm excitation. In previous work, it was demonstrated that neuronal and vascular network can be imaged simultaneously at wavelengths at 1300 nm leveraging resonant enhancement of fluorophore, where one fluorophore must be excited to higher energy levels, this requires the fluorophore to have relatively high, blue-shifted absorption cross-section [21]. Herein, we aim to propose a generalized strategy to allow simultaneous imaging of neurons and vasculature pushing the imaging depth even further with excitation at around 1700nm combining a 2-photon and 3-photon fluorescence probe pair, for which the RFP with absorption maximum around 550 nm as the 3-photon excited probe, and the cyanine derivative dye Q820@BSA with absorption maximum around 825 nm as the 2-photon excited probe. The peaks of the emission spectra have over 250 nm separation, open the door to a wide spectral range for potential future work on color multiplexing to label cell-type specific neurons. The 2-photon action cross-section of Q820@BSA was found to be about 2-fold larger than that of ICG at the excitation wavelength of around 1700nm. A through-white-matter brain vessel image was achieved as deep as 1.7 mm via the dye Q820@BSA, and simultaneous neurovascular imaging at depth was achieved up to 1.2-1.3 mm via such proposed fluorescent probe pair.

Biomedical Optics EXPRESS

2. Methods

2.1. Materials

All reagents and solvents were used as received without further purification. Bovine serum albumin (BSA) (98%) was purchased from Sigma-Aldrich (St. Louis, USA). ICG and all other chemicals were bought from Aladdin (Shanghai, China). The extracted RFP [22] was a donation from a biosynthetic lab to characterize its optical properties (Fig. 2). The RFP was also expressed in the transgenic mice for labeling neurons (also see Method: Animal preparation and *in vivo* imaging).

2.2. Preparation of Q820 and Q820@BSA

The synthesis of Q820 was based on the cyanine dye preparation procedure based on our previous work [23]. Briefly, compound A was first synthesized by mixing 1,1,2-trimethyl-1H-benzo[e]indole (1.05 g, 5.0 mmol) in toluene (10 mL), EtI (0.48 mL, 6.0 mmol) under argon atmosphere. The reaction mixture was stirred under reflux overnight, then allowed to cool to room temperature. The solvent was removed under vacuum filtration and the residue was washed with ether to afford the desired product 12 (1.5 g, 82%) as a blue solid. To a solution of compound A (182.5 mg, 0.5 mmol) in EtOH (10 mL), sodium acetate (41 mg, 0.5 mmol) and N-((E)-(2-chloro-3-((E)-(phenylimino)methyl)cyclohex-2-en-1-ylidene)methyl)aniline hydrochloride (90 mg, 0.25 mmol) was added gradually under argon atmosphere. The reaction mixture was stirred under reflux for 4 h, then allowed to cool to room temperature. After evaporation of solvent, the residue was purified by flash chromatography. The ^{1}H NMR results for the molecular characterization of the Q820 (measured at 400 MHz in $CDCl_3$) are as follows: δ 8.47 (doublet, J = 14.1 Hz, 2 H), δ 8.15 (doublet, J = 8.5 Hz, 2 H), δ 7.96 (apparent triplet, J = 8.2 Hz, 4 H), δ 7.67-7.59 (multiplet, 2 H), δ 7.52-7.44 (multiplet, 4 H), δ 6.23 (doublet, J = 14.1 Hz, 2 H), δ 4.31 (triplet, J = 7.0 Hz, 4 H), δ 2.76 (triplet, J = 5.4 Hz, 4 H), δ 2.10-2.00 (multiplet, 14 H), δ 1.95-1.85 (multiplet, 4 H), δ 1.54-1.45 (multiplet, 4 H), δ 1.42-1.35 (multiplet, 4 H), δ 1.32-1.22 (multiplet, 52 H), and δ 0.87 (triplet, J = 6.7 Hz, 6 H). The molecular structure of Q820 was shown in Supplement 1 as Supplement 1 Figure S1.

We prepared Q820@BSA for prolonging the retention time of Q820 in the blood, using the following protocol: 100 µL of Q820 in DMSO solution (10 mg/mL) was added drop by drop into 4 mL of BSA in 1x PBS solution under vortexing (with a mass ratio of 1:100 between Q820 and BSA). The resulting solution was gently shaken overnight at room temperature. Finally, the DMSO was removed by centrifugal filtration (Amicon 10 kDa) at 7000 rpm. The residue was washed three times with 1x PBS. The final solution was adjusted to 5 mL and passed through a 0.22 µm syringe filter for further use.

2.3. Spectrum measurement

All the absorption and emission spectra were measured in our lab. The UV to visible absorption spectra were recorded on UV-2700 Spectrophotometer (SHIMADZU, Japan). The fluorescence emission spectra were measured by Edinburgh Instruments FLS920.

2.4. Imaging setup

Figure 1 shows the schematic of our imaging system and excitation schemes for the demonstrated experiments. We used a wavelength-tunable optical parametric amplifier (OPA, Opera-F, Coherent) pumped by an amplifier (Monaco, Coherent) for multi-photon excitation. The laser was operated at 1650 nm. Between the imaging depths of 0-1200 µm, we used a laser repetition rate of 1 MHz. In Figs. 3 –5, the power used before reaching the white matter layer, which appears around 900 µm depth, was 21 mW. After crossing the white matter, the power was increased to 42 mW. The increased background observed in the 2-photon fluorescence channel is likely due to

Biomedical Optics EXPRESS

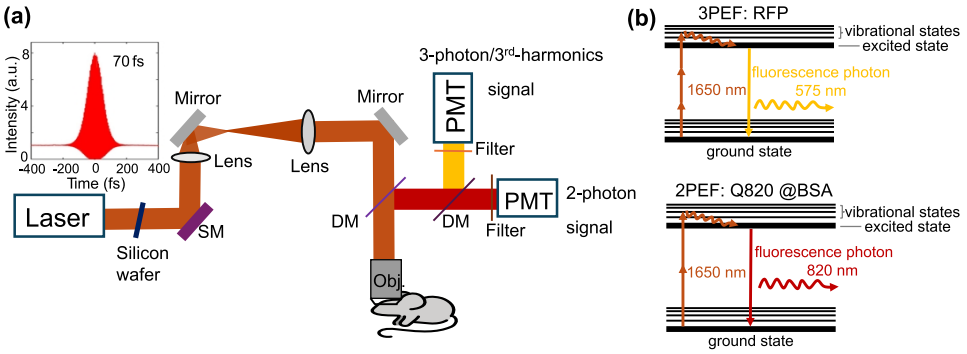

Fig. 1. Imaging setup and 2-photon and 3-photon excitation schemes at 1650 nm for simultaneous imaging of neurovascular structures. (a) A laser (OPA, Opera-F, Coherent), pumped by an amplifier (Monaco, Coherent), is directed into a multiphoton imaging system (Movable Objective Microscope, Sutter Instrument). Before entering the system, a 3-mm thick silicon wafer is used to compensate for the dispersion of our imaging system. The pulse's full width at half maximum (FWHM) is ~70 fs after the objective assuming a sech2(τ) temporal pulse intensity profile. SM: scanning mirrors; DM: dichroic mirrors. Details on the setup are described in the methods section: imaging setup. (b) Simultaneous 1650 nm 3-photon excitation of red fluorescent protein (RFP tdimer2(12)) for labeling neurons and 2-photon excitation of Q820@BSA for labeling vasculature in the brain *in vivo*.

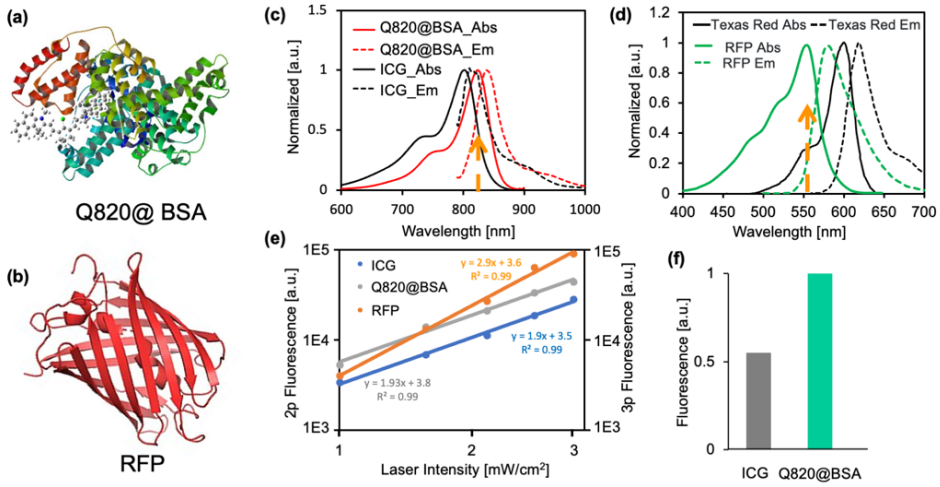

Fig. 2. (a) The molecular geometry of Q820@BSA. (b) The molecular geometry of RFP. (c) Absorption and emission spectra of ICG and Q820@BSA. (d) Absorption and emission spectra of RFP and Texas Red. (e) (left axis) The 2-photon fluorescence intensity as a function of excitation laser intensity of ICG and Q820@BSA; (right axis) the 3-photon fluorescence intensity as a function of excitation laser intensity of RFP. All axes were in log scale. The fitting functions, fitting coefficients, and goodness of fit (R^2) have been displayed. (f) The normalized multiphoton fluorescence of ICG and Q820@BSA (2-photon) with excitation at 1650 nm.

both this power increase and the increased scattering from the white matter. To ensure a fair comparison of signal decay across different depths, we normalized the square of the power for 2-photon fluorescence and the cubic square of the power for 3-photon fluorescence or THG at each depth when plotting the fluorescence and THG signal decay curves. Beyond 1200 μm and up

Biomedical Optics EXPRESS

to 1800 µm, we used a laser repetition rate of 500 kHz, with a maximum power of 50 mW under the objective. We reduced the laser repetition rate from 1 MHz to 500 kHz for deeper imaging to balance the trade-off between excitation efficiency and tissue heating. As imaging depth increases, higher pulse energy is required to generate sufficient signal due to increased scattering and absorption in brain tissue. Lowering the repetition rate allows us to increase the pulse energy without exceeding the maximum allowable average power (estimated conservatively at 50 mW), helping to avoid potential thermal damage while maintaining high excitation efficiency for deep tissue imaging [24]. A laser scanning microscope (Movable Objective Microscope, Sutter Instrument) was used. A silicon wafer was inserted in the beam path to compensate the dispersion in the system [25]. To collect fluorescence emission, we employed different combinations of filters. For Q820@BSA emission, we used a 800-nm long-pass filter (Thorlabs, FELH0800) and a band-pass filter (Semrock, FF01-889/42-25, with over 93% transmittance for wavelengths between 867.5 and 909.5 nm). For RFP or Texas Red emission, we used a 593-nm long-pass filter (Semrock, FF01-593/LP-25) in combination with a band-pass filter (FF01-630/92-25), which provides over 93% transmittance for wavelengths between 584 and 676 nm. For the third-harmonic signal collection, a 558 ± 10 nm bandpass filter (Semrock) was used. For the detection of the third-harmonic/3-photon fluorescence signal, a GaAsP photomultiplier tube (H7421-40, Hamamatsu Photonics) was used. For the detection of the Q820@BSA fluorescence signal, a GaAs photomultiplier tube (H7421-50, Hamamatsu) was used. Current generated by the PMT was converted to voltage (0.1 VµA-1) and low-pass-filtered (20kHz) by a transimpedance amplifier (C7319, Hamamatsu Photonics). Analog-to-digital conversion was performed by a data acquisition card (NI PCI-6110, National Instruments. We use a custom high NA water immersion microscope objective (XLPLN25XWMP2, Olympus, 25× 1.05 NA) with coating for high transmission (~80%) at 1,650 nm. A dichroic mirror (750DCXXR, Chroma Technology) was used to direct the fluorescence and third harmonic signal to the PMTs.

2.5. Animal preparation and in vivo imaging

Animal procedures were reviewed and approved by the Cornell Institutional Animal Care and Use Committee. We used male wildtype mouse (C57BL/6J, 8 weeks old, Jackson Laboratory) for Q820@BSA labelled vasculature imaging, and B6.Cg-Tg(Thy1-Brainbow1.0) HLich/J mice (18 g, 8 weeks old, The Jackson Laboratory) for RFP-labelled neuronal imaging. The B6.Cg-Tg(Thy1-Brainbow1.0) HLich/J mice were not subjected to Cre recombinase, so the only fluorescent protein expression was from RFP tdimer2(12). Craniotomy was performed on an 8-week-old mouse centered at 2 mm posterior and 2 mm lateral to the Bregma point. The cranial window with a circular shaped glass of 5 mm in diameter was mounted directly on the intact dura during imaging. The mouse was immediately imaged after craniotomy and was anesthetized with isoflurane (1-2% in oxygen for induction and 1.5-2% for surgery and imaging to maintain a breathing rate of 1 Hz). During the *in vivo* imaging session, the mouse body temperature was maintained at 37.5 °C with a temperature- controlled blanket (Harvard Apparatus) and the eyes were kept lubricated with eye ointment. Heavy water (D_2O) was used as the immersion medium to minimize the absorption of the excitation wavelength at 1650 nm.

For imaging of the vasculature in the mouse brain *in vivo*, the dye was retro-orbitally injected for labeling. The Q820@BSA injection dose is based on the mouse's weight, typically 10 mL/kg. In our study, the dose was approximately 0.2 mL. The maximum optical power at the surface of the mouse brain was around 50 mW for the deepest imaging. All images were taken at a frame rate of 0.24 Hz (512 × 512 pixels/frame) with a field of view (FOV) of 340 × 340 µm. At the largest depth, the frame was averaged 25 times. For imaging depth measurement, because the reported imaging depths are based on the raw axial movement of the objective, the slightly larger index of refraction in brain tissue relative to water resulted in a slight underestimate (5–10%) of the actual imaging depth within the tissue [13].

Biomedical Optics EXPRESS

To calibrate the laser power for coupling 2-photon and 3-photon excitation using a single long-wavelength light source, we first measured the fluorescence response of RFP and Q820@BSA at an excitation wavelength of 1650 nm across a range of laser powers. This allowed us to confirm the nature of excitation by analyzing how fluorescence intensity depended on laser power. Specifically, we plotted fluorescence versus laser power on a log-log scale and examined the slopes of these plots (Fig. 2(e)). The slope analysis revealed that RFP undergoes 3-photon excitation, while Q820@BSA undergoes 2-photon excitation, confirming the expected multiphoton processes at 1650 nm. For *in vivo* imaging in mouse brains, we further calibrated the laser power at different tissue depths. This was done by estimating the power at the focal point based on the surface power measurement and accounting for power decay over the effective attenuation length. We then adjusted the laser power within a suitable range to ensure expected multiphoton excitations.

3. Results

3.1. Characterization of RFP, ICG and Q820@BSA

We used RFP to label the neurons (see details in Methods part), the RFP (tdimer2 (12)) has an absorption peak around 550 nm, and therefore to excite 3-photon fluorescence efficiently, the excitation wavelength was chosen around 1650 nm (Fig. 2(d)). To perform 2-photon fluorescence imaging of the vasculature with the same excitation wavelength with efficient 2-photon excitation, a Q820 dye was synthesized (see method), whose absorption peak was approximately 825 nm. To obtain a well-biocompatible fluorescent probe and prolong the circulation time of Q820 in the blood, the Q820 was incubated first with BSA to form a Q820@BSA complex (Fig. 2(a)). The circulation time of Q820@BSA in the blood is quantified in Supplement 1 Figure S2 to be around 2 hours in half life. The absorption and emission spectra of Q820@BSA, ICG and RFP (tdimer2 (12)) were shown in Fig. 2(c) and 2(d). The maximum absorption of Q820@BSA is around 825 nm which is about 40 nm redshifted from that of ICG (785 nm). For the RFP (tdimer2 (12)), the maximum absorption is around 550 nm. We chose an excitation wavelength around 1650 nm for efficient 2-photon excitation of Q820@BSA and the 3-photon excitation of RFP. The 2- and 3-photon fluorescence intensity as a function of the excitation laser intensity with excitation at 1650 nm was shown in Fig. 2(e). A slope around 2 for both Q820@BSA and ICG fluorescent and about 3 for RFP was validated indicating a pure 2- and 3-photon excitation regime. The normalized 2-photon fluorescence of ICG and Q820 was shown in Fig. 2(f). For ICG and Q820@BSA at the same molecular concentration (1 μM), the corresponding 2-photon fluorescence intensity was found to be about 2 folds larger for Q820@BSA than ICG at excitation of 1650 nm. The larger spectral separation (~250 nm between peaks of the emission spectra) between RFP and Q820@BSA effectively avoids spectral crosstalk, opening a large spectral window for potential multiplexed imaging of various fluorophores excitable with 2-photon and 3-photon excitation at 1700nm. Meanwhile, the enhanced brightness allows for 30% reduced power needed for 2-photon excitation of Q820@BSA compared with ICG to provide images at the same brightness, making intravital imaging more feasible.

3.2. Deep in vivo 2-photon fluorescence imaging of vasculature in the mouse brain

To validate the performance of Q820@BSA for mouse brain imaging, we perform 2-photon fluorescence imaging of the brain vasculature via retro-orbital injection of Q820@BSA and with fluorescence excitation about 1650 nm. A 3D image stack was acquired and reconstructed for the 2-photon fluorescence channel as shown in Fig. 3(a). While 2-photon fluorescence excitation is being performed, other light-matter interactions, such as third-harmonic generation (THG), also occur in a label-free manner. The THG processes produce signals that are proportional to the nonlinear index mismatch arising from different interfaces within the brain, such as the lipid-water interface. We simultaneously collect the label-free THG signal with the long-wavelength-excited

Biomedical Optics EXPRESS

2-photon fluorescence in the brain. During the first few hundreds of microns deep in the cortical layers, the THG contrast is mainly due to lipid-rich structures such as blood vessels and myelinated axons. Through THG imaging, the white matter could be clear distinguished with the characterized pattern of the filaments from 875 µm to 950 µm as shown in Fig. 3. THG signal is degraded when imaging deeper. After the whiter matter layer is reached, there is a significant drop in THG signal, and a stronger background is visible in the 2-photon fluorescence channel as a result of the increased scattering from white matter layers. Despite strong scattering, we were still able to visualize blood vessels at the depth around 1700 μm.

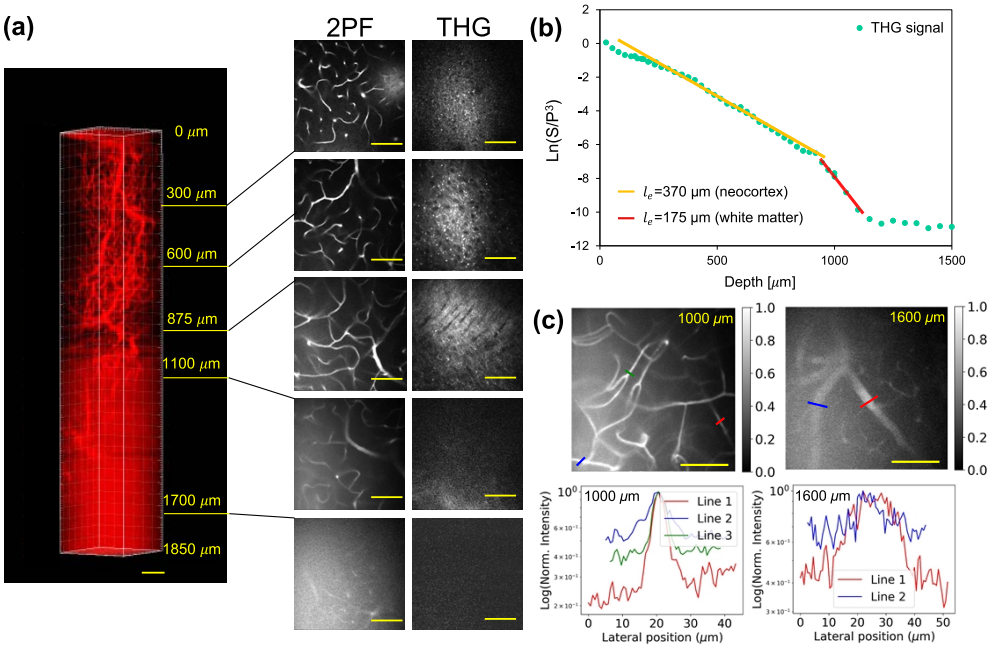

Fig. 3. Deep brain vasculature imaging with Q820@BSA labeling. (a) The 3D reconstruction of the brain vasculature via 2-photon fluorescence imaging with excitation at 1650 nm, and the corresponding third-harmonic generation (THG) images with scale bar at 100 μm. The scale bar is 100 µm. (b) THG signal decay curve plotted on a semi-log scale for calculating the effective attenuation lengths in the neocortex and the white matter layer. The straight lines are linear fitting results for calculating the effective attenuation length l_e. The effective attenuation length measured from THG signal is around 370 μm in neocortex and 175 μm in the white matter area. (c) Quantification of the signal-to-background ratios in deep 2-photon fluorescence images over 1 mm. Upper panel: Normalized images at 1000 μm and 1600 μm depths. (Left) 2-photon fluorescence image of a brain vessel at 1000 μm depth; (Right) 2-photon fluorescence image of a brain vessel at 1600 μm depth. Lower panel: Line profiles of the normalized signals along the colored lines shown in the upper panel, with the y-axis in log scale. The scale bar is 100 μm.

We quantified the signal-to-background ratios (SBRs) at various locations in Fig. 3(c). By plotting line profiles of various blood vessel features at different background levels, we were able to calculate the SBRs, where the signal is defined as the peak intensity of the blood vessel minus the mean intensity of the surrounding tissue background, and the background is the mean intensity of the surrounding tissue. At the depth of 1000 μm, the SBR ranges from 1 to 4; at 1600 μm, it ranges from 0.75 to 1.75 (Fig. 3(c)). It is also clearly shown in the images that high-resolution capillaries are still visible with 2-photon vasculature imaging with Q820@BSA at 1650 nm excitation.

Biomedical Optics EXPRESS

3.3. Quantitative comparison of signal decay of 2-photon excited Q820@BSA and 3-photon excited Texas Red at the same 1700nm window

To quantitatively evaluate and compare the long-wavelength 2-photon probe with the 3-photon probe (using Texas Red as the labeling agent) under the same excitation wavelength, we characterized the optical properties of the brain tissue by comparing the signal attenuation curves of 2-photon and 3-photon fluorescence signal decay using the effective attenuation length. In Fig. 4, 2-photon and 3-photon fluorescence signal as a function of image depth was analyzed. Each image's signal was calculated as the average value of the top 0.1% of all pixels. The natural logarithm of signal normalized by cubic square of power used at the brain surface S/P^3 as a function of the imaging depth for 3-photon fluorescence and natural logarithm of signal normalized by square of power used at the brain surface S/P^2 as a function of the imaging depth was shown in Fig. 4. In a heavily scattering tissue environment, the intensity of the excitation beam at the focus would be greatly reduced as a function of imaging depth. In this analysis, all imaging was done in the same brain region within the same mouse, with the only difference being the fluorescence probes, which have two distinct emission wavelengths. The $\ln\left(\frac{S}{P^m}\right)$ as a function of the imaging depth could be described as Eq. (1), where P is the power used at the brain surface for each imaging depth, m is the order of nonlinear process, and l_e is effective attenuation length. The constant C includes factors such as the fluorophore's absorption cross section, the system detection efficiency, the concentration of the fluorescent dye, and any other system-dependent parameters like the collection optics and quantum efficiency of the detector:

$$\ln\left(\frac{S}{P^m}\right) = C - ml/l_e \ . \tag{1}$$

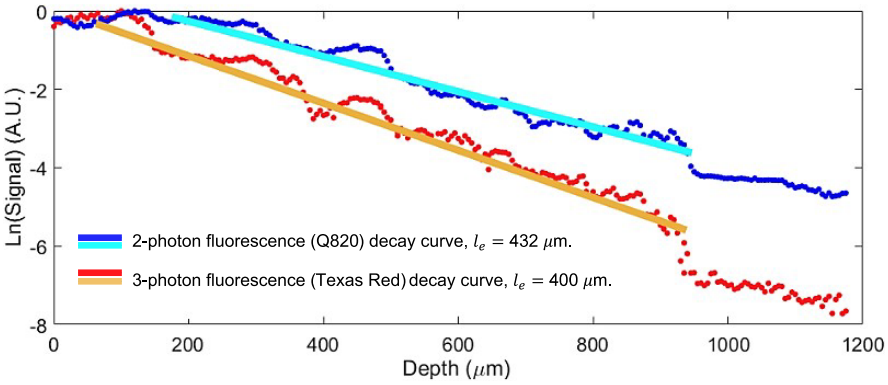

Fig. 4. 2-photon and 3-photon fluorescence signal decay curve plotted on a semi-log scale for calculating the effective attenuation lengths in the neocortex. The straight lines are linear fitting results for calculating the effective attenuation length l_e. The irregular bumpy structure seen in both the 2P and 3P plots is likely due to the inhomogeneity of vasculature, specifically the presence of large blood vessels that cross through different cortical depths. This variability in vasculature can create uneven signal intensities at various depths, leading to the observed irregularities in the plots.

A clear turning point could be observed at the depth around 900 m in Fig. 4. According to Eq. (1), the change in the slope corresponds to the variation of the effective attenuation length l_e. It is consistent with the adult mouse brain anatomy that the low scattering somatosensory cortex has a thickness of about 1 mm, and beyond that the high scattering white matter is present. Under the white matter lies the hippocampus region. The l_e of cortex was found to be around 400 μm for 3-photon fluorescence with shorter emission wavelength (Texas Red) while for the

Biomedical Optics EXPRESS

attenuation length is around 432 μm for 2-photon fluorescence with longer emission wavelength (Q820@BSA).

Previously, it was observed that the impact of emission wavelength on multiphoton imaging depth is negligible within the superficial 1 mm of the mouse brain [26]. Here, we demonstrate that when the emission wavelengths are significantly different (~250 nm), we can observe a relatively small but positive impact on the effective attenuation length (increase of 8% in effective attenuation length when shifting to longer wavelength). This observation aligns well with previous work and motivates us to explore the 1700nm excitation window with long emission wavelength, which has the benefits of the longer attenuation length from the excitation and emission, for multi-color imaging and deep tissue imaging.

3.4. *Simultaneous deep neuron and vasculature imaging within living intact mouse brain*

Although previous work has shown simultaneous multi-color imaging of neurons and vasculature with 3-photon excitation, it either requires complicated custom laser sources or a specific excitation scheme [21,27]. For deeper imaging, longer excitation wavelengths of 1700nm are preferred. It should be noted, however, that *in vivo* imaging in the 1700nm window is limited by the availability of bright and biocompatible fluorophores. As part of our research, we synthesized and applied Q820@BSA probes for labeling mouse vasculature. Using excitation around 1650 nm, deep 2-photon imaging was possible through white matter, as demonstrated above. Moreover, the 3-photon photon excitation of RFP occurs within the same excitation region. To simultaneous image neurovascular network at depth, we simultaneously excited Q820-RFP probe pairs with 2-photon excitation and 3-photon excitation at 1650 nm with excitation scheme shown in Fig. 1(b). The average power we used in the deepest region is 50 mW under the objective with 500 kHz laser repetition rate. By simultaneous 2-photon excitation of Q820@BSA for vasculature imaging and 3-photon excitation of RFP for neuronal imaging, we are able to exploit fully the excitation wavelength advantage in the 1700nm imaging window for deep brain imaging. In Fig. 5, we demonstrate simultaneous deep neurovascular imaging in the living adult mouse brain, penetrating highly scattering white matter and reaching deep into the hippocampus.

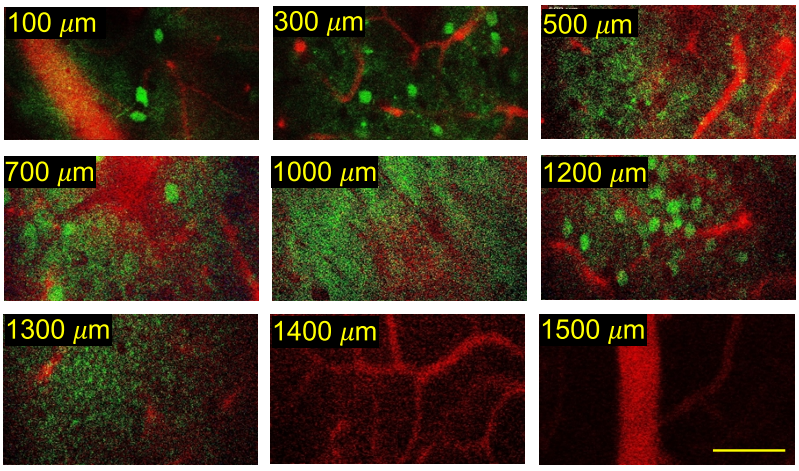

Fig. 5. The neurovascular imaging of *in vivo* adult intact mouse brain at 1650 nm excitation with 2-photon fluorescence for Q820@BSA labeled blood vessels and 3-photon fluorescence for RFP labeled the neurons. At a depth of 1000 μm, white matter is observed, and we can go beyond the dense neurons in the hippocampus layer observed at 1200 μm. Scalar bar: 100 μm.

Biomedical Optics EXPRESS

Clear vessels could be seen much deeper due to the bright Q820@BSA probe, up to 1500 μm, through the highly scattering white matter layers, as shown in Fig. 5. The imaging depth for RFP-labeled neurons is limited by the brightness and sparseness of the RFP variant we employed. While clear visualization of neurons is achievable up to 1.2 mm, the signal quality significantly decreases beyond 1.3 mm. However, this limitation is not inherent to the technique itself, but rather due to the specific properties of the RFP used in our experiments. Recent advancements in red-shifted fluorescent proteins, such as mScarlet and other enhanced RFPs, have demonstrated significantly improved brightness and photostability, which could potentially extend the imaging depth in future studies [28,29]. These newer variants may allow us to push the imaging depth by an additional 0.3-0.4 mm.

Compared to previous work based on 1300 nm excitation for multicolor 3-photon imaging [21], our approach using 1700nm excitation is relatively more universal, as it can be potentially applied to a range of 2-photon and 3-photon probes with excitation peaks around half or one-third of 1700nm. Our design does not require the fluorophores to have the relatively high, blue-shifted absorption cross-section required in previous work [21]. Moreover, our design offers several potential key advantages. The longer wavelength not only reduces scattering, enabling deeper tissue penetration (another 0.3-0.4 mm deeper in principle, demonstrated partially by deep 2-photon vasculature imaging in this work), but also allows for the use of fluorophores with larger spectral separations (~250 nm), allowing for potentially highly multiplexed imaging across broad spectral ranges from visible to near-infrared.

Our approach could be particularly beneficial for studying deep neurovascular coupling, as it provides clearer separation of signals from different probes, reducing spectral crosstalk and enhancing image clarity in highly scattering brain tissues. Additionally, our design offers a flexible platform for exploring various fluorophore designs and excitation schemes for deep brain imaging. One example would be exploring resonance-enhanced three-photon excitation [21] as a complementary excitation scheme for multiplexed imaging at 1700nm.

4. Conclusion

The ability to image the neurovascular network in the intact mouse brain holds considerable scientific interest due to its importance in supporting and regulating neuronal activity. Deep imaging of these structures is pivotal as they play critical roles, including nutrient transport, waste removal, and overall neuronal health maintenance. Non-invasive, high-resolution imaging of these deep-lying structures in intact mouse brains can yield invaluable insights into the physiological and pathological processes related to neurovascular coupling. In this study, we have introduced a neurovascular probe pair, RFP and Q820@BSA, by matching the transition energy between the 3-photon excitation of RFP and the 2-photon excitation of Q820@BSA, we are able to conduct *in vivo* simultaneous 2- and 3-photon fluorescence structural imaging of neurovascular through the highly scattering white matter in an adult mouse brain excited at the same wavelength. Our investigations also suggest a potentially high 2-photon action cross-section for Q820@BSA, enabling the capture of deep vascular labelling images extending to a depth of 1700 μm beyond the white matter. We anticipate further efforts to be made to develop brighter red fluorescent proteins to enable the imaging of the neurovascular system at greater depths.

Our findings underscore the potential for simultaneous imaging of neuronal cells and brain vessels using 3-photon and 2-photon mechanisms at the same excitation wavelength, particularly at 1700nm, a method that could be broadly applicable due to its inherent generalizability. This method not only streamlines the imaging process but also minimizes potential tissue damage from multiple excitation wavelengths. We hope it provides methodological foundation for future *intravital* studies investigating neurovascular interactions in deeper brain tissues and stimulates further development of advanced fluorescent probes that are bright, biocompatible, and capable of emitting far-red and near-infrared (NIR) fluorescence for targeted labeling of neurovascular

Biomedical Optics EXPRESS

system. The advancement of these tools can improve our capacity to explore the complex interactions within the brain's neurovascular network, thereby deepening our understanding of its function and contributing to potential strategies for addressing neurological disorders.

Funding. Natural Science Foundation of Shenzhen Municipality (JCYJ20200109115633343); National Natural Science Foundation of China (22077135, 22377142).

Acknowledgments. We thank Dr. Chris Xu for providing the imaging setup for part of the experiments.

Z.C., X.G. and Q.S. acknowledge funding support from Natural Science Foundation of Shenzhen Municipality (JCYJ20200109115633343) and National Natural Science Foundation of China (22077135,22377142).

Disclosures. The authors claim no conflict of interest.

Data availability. Data of the results are available under reasonable request from the corresponding authors.

Supplemental document. See Supplement 1 for supporting content.

References

1. L. Kaplan, B. W. Chow, and C. Gu, "Neuronal regulation of the blood-brain barrier and neurovascular coupling," Nat. Rev. Neurosci. **21**(8), 416–432 (2020).
2. T. Takano, G. F. Tian, W. Peng, *et al.*, "Astrocyte-mediated control of cerebral blood flow," Nat. Neurosci. **9**(2), 260–267 (2006).
3. M. Vanlandewijck, L. He, M. A. Mäe, *et al.*, "A molecular atlas of cell types and zonation in the brain vasculature," Nature **554**(7693), 475–480 (2018).
4. M. D. Sweeney, A. P. Sagare, and B. V. Zlokovic, "Blood-brain barrier breakdown in alzheimer disease and other neurodegenerative disorders," Nat. Rev. Neurol. **14**(3), 133–150 (2018).
5. E. M. C. Hillman, "Coupling mechanism and significance of the BOLD signal: a status report," Annu. Rev. Neurosci. **37**(1), 161–181 (2014).
6. P. O'Herron, P. Y. Chhatbar, M. Levy, *et al.*, "Neural correlates of single-vessel haemodynamic responses in vivo," Nature **534**(7607), 378–382 (2016).
7. J. H. Lee, R. Durand, V. Gradinaru, *et al.*, "Global and local FMRI signals driven by neurons defined optogenetically by type and wiring," Nature **465**(7299), 788–792 (2010).
8. C. A. Combs "Fluorescence microscopy: a concise guide to current imaging methods," Curr. Protoc. Neurosci. 2010, No. SUPPL. 50, 1–19.
9. D. Herrmann, D. Entenberg, C. Celso, *et al.*, "Multiphoton intravital microscopy of rodents," Nature Rev. **2**, 89 (2022).
10. D. Kobat, N. G. Horton, and C. Xu, "*In vivo* 2-photon microscopy to 1.6-mm depth in mouse cortex," J. Biomed. Opt. **16**(10), 1 (2011).
11. F. Xia, M. Gevers, A. Fognini, *et al.*, "Short-wave infrared confocal fluorescence imaging of deep mouse brain with a superconducting nanowire single-photon detector," ACS Photonics **8**(9), 2800–2810 (2021).
12. G. Hong, S. Diao, J. Chang, *et al.*, "Through-skull fluorescence imaging of the brain in a new near-infrared window," Nat. Photonics **8**(9), 723–730 (2014).
13. N. G. Horton, K. Wang, D. Kobat, *et al.*, "*In vivo* 3-photon microscopy of subcortical structures within an intact mouse brain," Nat. Photonics **7**(3), 205–209 (2013).
14. T. Wang, D. G. Ouzounov, C. Wu, *et al.*, "3-photon imaging of mouse brain structure and function through the intact skull," Nat. Methods **15**(10), 789–792 (2018).
15. Z. Chang, F. Liu, L. Wang, *et al.*, "Near-infrared dyes, nanomaterials and proteins," Chin. Chem. Lett. **30**(10), 1856–1882 (2019).
16. A. E. Palmer, X. Shu, J. Zhang, *et al.*, "The growing and glowing toolbox of fluorescent and photoactive proteins," Trends Biochem. Sci. **42**(2), 111–129 (2017).
17. H. Cheng, S. Tong, X. Deng, *et al.*, "Deep-brain 2-photon fluorescence microscopy *in vivo* excited at the 1700nm window," Opt. Lett. **44**(17), 4432 (2019).
18. M. Wang, C. Wu, D. Sinefeld, *et al.*, "Comparing the effective attenuation lengths for long wavelength *in vivo* imaging of the mouse brain," Biomed. Opt. Express **9**(8), 3534 (2018).
19. F. Xia, C. Wu, D. Sinefeld, *et al.*, "*In vivo* label-free confocal imaging of the deep mouse brain with long-wavelength illumination," Biomed. Opt. Express **9**(12), 6545–6555 (2018).
20. Y. Hontani, N. Akbari, K. E. Kolkman, *et al.*, "Deep-tissue three-photon fluorescence microscopy in intact mouse and zebrafish brain," J. Visualized Exp. **179**(179), e63213 (2022).
21. Y. Hontani, F. Xia, and C. Xu Multicolor 3-photon Fluorescence Imaging with Single-Wavelength Excitation Deep in Mouse Brain (2021), Vol. 7, http://spectra.arizona.edu/.
22. R. E. Campbell, O. Tour, A. E. Palmer, *et al.*, "A monomeric red fluorescent protein," Proc. Natl. Acad. Sci. **99**(12), 7877–7882 (2002).
23. Zong Chang, Chenchen Liu, Like Guo, *et al.*, "Single-dye NIR-II chemiluminescence system for H2O2 imaging," Chem. Commun. **59**(41), 6171–6174 (2023).
24. T. Wang and C. Xu, "3-photon neuronal imaging in deep mouse brain," Optica **7**(8), 947–960 (2020).

Biomedical Optics EXPRESS

25. N. G. Horton and C. Xu, "Dispersion compensation in 3-photon fluorescence microscopy at 1,700 Nm," Biomed. Opt. Express **6**(4), 1392 (2015).
26. M. Wang, M. Kim, F. Xia, *et al.*, "Impact of the emission wavelengths on *in vivo* multiphoton imaging of mouse brains," Biomed. Opt. Express **10**(4), 1905–1918 (2019).
27. K. Guesmi, L. Abdeladim, S. Tozer, *et al.*, "Dual-color deep-tissue 3-photon microscopy with a multiband infrared laser," Light: Sci. Appl. **7**(1), 12 (2018).
28. Theodorus W. J. Gadella Jr., Laura van Weeren, Jente Stouthamer, *et al.*, "mScarlet3: a brilliant and fast-maturing red fluorescent protein," Nat. Methods **20**(4), 541–545 (2023).
29. D. S. Bindels, L. Haarbosch, L. Van Weeren, *et al.*, "mScarlet: a bright monomeric red fluorescent protein for cellular imaging," Nat. Methods **14**(1), 53–56 (2017).